Rotational and Translational Dynamics of Rodlike Polymers: A Combined Transient Electric Birefringence and Dynamic Light Scattering Study

J. K. Phalakornkul,† A. P. Gast,† and R. Pecora*,‡

Chemistry and Chemical Engineering Departments, Stanford University, Stanford, California 94305

Received October 21, 1998; Revised Manuscript Received February 19, 1999

ABSTRACT: Dynamic light scattering (DLS) and transient electric birefringence decay measurements are performed on poly(γ-benzyl-α-L-glutamate) solutions over a wide concentration range. We interpret the primary dynamic decay rate always observed from dynamic light scattering experiments by extending the expression for the decay rate beyond the original limits of the mean field (DSO theory) theory of Doi, Shimada and Okano, (*J. Chem. Phys.* **1988**, *88*, 4070) to more general time and length scales. Our result, expressed as a power series in the scattering vector magnitude q, shows that, as expected, the primary decay rate from dynamic light scattering experiments at small q directly provides diffusion coefficients for mutual translation, whereas that at larger q contains contributions from both rotation and translation, including terms containing the translational anisotropy. The rotational relaxation times are obtained independently from the transient electric birefringence experiments and are used in our formula to extract concentration dependencies of the self-diffusion coefficients from the DLS time correlation functions at large scattering vector q. Finally, from the data at large q, we report the transverse and longitudinal translational self-diffusion coefficients as functions of concentration.

1. Introduction

Systems containing rigid rodlike polymers have gained much attention in recent years because of both their important technological applications and their status as the simplest model for entangling polymers.[1,2] Understanding the dynamic behavior of flexible polymer molecules is not an easy task. The complexity arises from the many degrees of freedom and the multiple types of interactions among the molecules and between different parts of the same molecule. The fact that rodlike polymers in a semidilute suspension exhibit only two types of motion, translation and overall rotation, is a great simplification in interpreting the dynamics of entangled polymers. Theoretical treatments of the dynamic properties of flexible and rodlike systems have originated from the same basic concepts and have evolved along parallel paths.

Systems of rodlike polymers, although relatively simple, still exhibit nontrivial dynamic behavior. In nondilute suspensions, this behavior is associated with three dominant molecular interactions. The "excluded volume" interaction is a static interaction which includes steric repulsion, van der Waals attraction, and solvent-mediated interactions. The entanglement interaction is purely geometrical in nature. The topological constraint that a polymer is connected in one dimension inhibits chain crossing and induces a strong correlation that can be interpreted as an apparent intermolecular interaction. The other major interaction is due to hydrodynamic friction forces. These interactions affect rotation, longitudinal translation (parallel to the long rod axis), and transverse translation (perpendicular to the long axis) of rodlike polymers. The simplest description of these motions is based on the tube model developed by Doi and Edwards (DE).[3,4] The polymer is modeled as an infinitely thin rod confined to a certain tubelike region bounded by neighboring rods. Motions of the confined rod depend on the motions of the rod itself and its caging neighbors.

In the semidilute regime, defined as $1/L^3 \leq n \leq 1/dL^2$ (n is the number concentration, L is the rod length, and d is the rod diameter), the original Doi−Edwards theory predicts that the rod rotation will be severely restricted. The dominant mechanism for the rotational relaxation is cage renewal whereby the caging becomes ineffective because of parallel translation of the test rod or because the cage breaks up by the translation of the rods that form the cage. Rotation is the result of the repetitive angular jumps characterized by the cage breakup and the frequency of the parallel translation. DE arrive at the following expression for the concentration dependence of the rotational diffusion coefficient D_r:

$$D_r/D_{ro} = \beta(nL^3)^{-2} \tag{1}$$

where D_{ro} is the value in the infinite dilution limit. Experimental investigations by electric birefringence[5−16] and depolarized light scattering[17] have indicated considerable discrepancies both in the detailed mechanism of the model and the onset concentration of the caging effects. Many studies attempt to make a quantitative refinement of the DE semiempirical theory to more rigorously explain the rod dynamics and bring theoretical prediction and experimental observation into agreement.[18,19] Of all of the modifications, the most important adjustment anticipates translation by part of the rod length instead of the full length as in the original DE model. These modified versions eliminate the large discrepancies but still disagree with what has been observed experimentally.[13,17] Recently, Fixman has asserted that two mechanisms are actually responsible for the rod rotation.[20,21] One is the cage renewal of Doi and Edwards. The other is due to the transverse translation

* To whom correspondence should be addressed.
‡ Chemistry Department.
† Chemical Engineering Department.

10.1021/ma981640d CCC: $18.00
Published on Web 04/13/1999

and rotation of both the caging rods and the test rod occurring before the longitudinal translation described in the DE theory takes over. On this time scale, the repulsion between the test rod and its neighbors results in transverse translation of the test rod and slight rotation of the neighbors away from the cage. At longer times, when the free energy associated with this rod−cage interaction decreases, such motions become less likely, and the rod escapes from the cage by the longitudinal translation of the DE theory. The Fixman theory provides very close agreement with experimental and simulation results of rigid rod rotation in the dilute and moderately high concentration regimes up to about 90 rods/L^3.[22,23] This theory provides a better understanding of the mechanisms behind the rotational mobility than previous theories based solely on simple caging.

In addition to the rotational dynamics, the DE theory also explores translational motions in the semidilute regime. Because the polymer is infinitely thin, the model assumes that a rod translates longitudinally as if it were in an infinitely dilute suspension. Motion in the perpendicular direction, on the other hand, is so restricted that it is conveniently approximated as being impossible. Consequently, the rod diffuses longitudinally independently of its surrounding neighbors. Perhaps the simplest experimental method of studying translational dynamics in these systems is light scattering.[17,24−26] The difficulty, however, is that the theoretical interpretation of the experimental dynamic light scattering (DLS) time correlation functions in terms of self-diffusion coefficients (both translational and rotational) is not yet well established in other than dilute solutions. DeLong and Russo employed dynamic light scattering measurements of the first cumulant[26] to reveal that the apparent translational diffusivity increases with scattering vector at low concentrations but decreases at higher concentrations.[26] Such phenomena were not well-understood until Doi, Shimada, and Okano (DSO) incorporated the three previously mentioned interactions in the mean field theory and their kinetic approach to calculate the dynamic structure factor that is measured in DLS.[24] The steric repulsion is considered directly by a pair potential, whereas the entanglement and hydrodynamic interactions are considered in adjustable self-diffusion coefficients. Hence, the DSO theory can be used to extract dynamic parameters of rigid polymers from the DLS correlation functions. Following the DSO theory, DeLong and Russo interpreted the change in the q-dependent apparent diffusivity with concentration as due to the dissimilar effects of the rotational relaxation at the macroscopic and microscopic limits.[26]

The basic approach of the DSO theory can serve as a basis for interpreting dynamic light scattering data of rodlike particles. DSO, however, carried out detailed calculations for the dynamic structure factor for only two specific experimental conditions: (1) For long probing length scales ($q \rightarrow 0$) at any time t and (2) For arbitrary length scales $1/q$ at short relaxation times ($t \rightarrow 0$). Although in the past few years, experimentalists have extended their interests to longer times over a whole range of accessible probing length scales, and have, consequently, probed more complex dynamics, the DSO final expression becomes inapplicable in these new regimes. The availability of inversion procedures seeking the optimal solution to multiexponential decay functions from data containing random noise assists in the analysis of the electric field autocorrelation functions obtained from DLS measurements.[27] However, a generally applicable physical interpretation of the different detected decay rates (dynamic modes) is still not available. A suitable theoretical description linking the DLS spectrum to the actual motions of the polymers is needed. Maeda extended the calculated dynamic structure factor beyond the original DSO limits for a more general time scale but did not put the expression for the function into a practical format. [28,29]

In this work, we attempt to interpret only the primary dynamic mode always observed in DLS experiments on dilute and nondilute suspensions of rodlike polymers. We do so by explicitly expressing the decay rate in terms of all of the characteristic diffusivities of the rods. Within the basic assumption of the DSO theory, our analytical expression indicates that extensive information on the polymer dynamics including cooperative diffusion, coupling between translational and rotational motions, and self-diffusion in perpendicular and parallel directions can be obtained from this dynamic mode. With this expression in hand, we analyze the DLS spectrum of the model system of poly-γ-benzyl-α-L-glutamate suspended in a good solvent to elucidate the dynamic behavior of the rods as they become more crowded.

Within the scope of the DSO theory, extracting the cooperative or mutual translational coefficient from the measured diffusivity is straightforward, but obtaining values of the self-diffusion coefficients is more complicated. For extraction of these self-diffusion coefficients, knowledge of rotational diffusion coefficients is a prerequisite. Previous work has identified the effects of rotation on the diffusivity measured by DLS both from a dilute suspension at long time[30] and a semidilute suspension at short time.[26,31] To our knowledge, there has never been a successful separation in the semidilute regime. The failure lies in the uncertainty in rotational mobilities experimentally measured by the depolarized light scattering technique.[17,25,32] Here, we utilize the transient electric birefringence technique (TEB), which is highly sensitive to the optical anisotropy of asymmetric molecules. In the TEB technique, we perturb molecules from their equilibrium orientation distribution with an externally applied electric field pulse. When a linearly polarized light beam passes through this optically anisotropic system, one of the light components is retarded. Rotational relaxation can be measured from the time dependence of the retardation. We characterize the rotation of the polymer as a function of concentration and length and compare the data with the existing theories[3,18] and simulations.[20,22,23] Using this knowledge of the rotational diffusion, we are able to extract the translational diffusivity and its anisotropy from the measured DLS relaxation rates. This methodology provides important insights into the self-diffusivities in the two directions. It must, of course, be kept in mind that the self-diffusivities obtained from the DLS depend on the validity of the original DSO theory and our extension of it.

In the following sections, we first describe in detail our calculation of the decay rate of the major dynamic mode mentioned above. Then, we discuss TEB measurements of the rotation of the rods in our suspensions. Following that, we apply our theoretical framework and our measured rotational mobilities to interpret the spectrum obtained from our DLS experiments. Finally,

we discuss the concentration dependencies of the various diffusion coefficients.

2. Dynamic Structure Factor

Our goal here is to calculate the primary decay rate of the dynamic structure factor $g(q, t)$ of rigid rodlike polymers in a semidilute suspension at an arbitrary scattering vector q and an arbitrary time t in a form that can be conveniently compared to dynamic light scattering measurements. Our calculation follows the DSO theory [24] but solves for the dynamic structure factor $g(q, t)$ by the perturbation method with higher order corrections to an eigenvalue problem, thereby resulting in terms of higher order in q than calculated by DSO. The coefficients of these terms, expressed as the cooperative translational diffusivity (D_t) and translational anisotropy (ΔD) are used to extract the concentration dependencies of each diffusive mode from the DLS spectrum.

The DSO theory starts with a kinetic equation for the average number concentration $f(\mathbf{r}, \mathbf{u}, t)$ of rods, in which the location of a rigid rod of length L and diameter d is represented by $\mathbf{r}$, the vector position of its center of mass, and $\mathbf{u}$, the unit vector along the long rod axis. In the dilute regime, the longitudinal friction force is greater than the transverse force; hence, the parallel coefficient in infinite dilution $D_{\|o}$ is larger than the perpendicular one $D_{\perp o}$. This diffusive anisotropy can induce an anisotropy in the orientational distribution (translational−rotational coupling). In a semidilute suspension, such coupling is expected to become more significant.[18] In the kinetic equation of DSO, the coupling between the translational and rotational diffusion is expressed by

$$\frac{\partial f}{\partial \mathbf{t}} = \frac{\partial}{\partial \mathbf{r}}[D_{\|}\mathbf{uu} + D_{\perp}(\mathbf{I} - \mathbf{uu})]\left[\frac{\partial f}{\partial \mathbf{r}} + \frac{f}{k_B T}\frac{\partial}{\partial \mathbf{r}}(h + \bar{W})\right] + D_r R\left[Rf + \frac{f}{k_B T}R(h + \bar{W})\right] \quad (2)$$

where the rotational operator R is $\mathbf{u} \times (\partial/\partial \mathbf{u})$. The potential h represents the influence of an external field on the polymer located at $(\mathbf{r}, \mathbf{u})$. The $\bar{W}(\mathbf{r}, \mathbf{u}, t)$ is the mean field approximation of the interaction potential $W(\mathbf{r} - \mathbf{r}', \mathbf{u}, \mathbf{u}')$ between the two polymers at $(\mathbf{r}, \mathbf{u})$ and $(\mathbf{r}', \mathbf{u}')$

$$\bar{W}(\mathbf{r}, \mathbf{u}, t) = \int d\mathbf{r}'\, d\mathbf{u}'\, W(\mathbf{r} - \mathbf{r}', \mathbf{u}, \mathbf{u}')f(\mathbf{r}', \mathbf{u}', t) \quad (3)$$

where, for thin rods, $W(\mathbf{r}-\mathbf{r}', \mathbf{u}, \mathbf{u}') = 1$ when the two rods overlap and is 0 otherwise.

The advantage of the mean field approximation is that the dynamic structure factor can be calculated from the kinetic equation, eq 2, without a knowledge of the pair distribution function. Three types of molecular interactions are taken into account in eq 2. The steric repulsion is directly represented by the pair potential, and the entanglement and hydrodynamic interactions are considered via the concentration dependent self-diffusion coefficients which are regarded as the adjustable parameters. DSO then apply the fluctuation−dissipation theorem and express the dynamic structure factor $g(q, t)$ in terms of the orthonormal eigenfunctions $\psi_{q,l}$ and $\psi^+_{q,l}$ and the eigenvalues $\lambda_{q,l}$ of the operators Ω_q and Ω^+_q

$$g(q, t) = 4\pi\frac{L}{c}\sum_l \frac{\langle \mathbf{s}_q|\psi_{ql}\rangle\langle\psi^+_{ql}|\theta_q \mathbf{s}_q\rangle}{\lambda_{ql}} \exp(-\lambda_{ql}t) \quad (4)$$

The inner product denoted by $\langle ... \rangle$ is defined as an integral of the product of the two functions.

$$\langle f|g\rangle = \frac{1}{4\pi}\int d\mathbf{u} f(\mathbf{u})g(\mathbf{u}) \quad (5)$$

The operator Ω_q expresses both the translational−rotational diffusion and the rod−rod interaction, whereas the operator θ_q considers only the self-translation and rotation according to the following equations:

$$\Omega_q f_q(\mathbf{u}, t)\,[D_{\|}(q\cdot\mathbf{u})^2 + D_{\perp}\{q^2 - (q\cdot\mathbf{u})^2\} - D_r R^2] \times \left[f_q(\mathbf{u}, t) + \frac{n}{4\pi}\int d\mathbf{u}'\, W_q(\mathbf{u}, \mathbf{u}')f_q(\mathbf{u}', t)\right] \quad (6)$$

$$\theta_q s_q(\mathbf{u}) = \frac{nL}{4\pi}[D_{\|}(q\cdot\mathbf{u})^2 + D_{\perp}\{q^2 - (q\cdot\mathbf{u})^2\} - D_r R^2]s_q(\mathbf{u}) \quad (7)$$

The thermal energy $k_B T$ in eq 6 is normalized to unity. The q component of the normalized electric field of the scattered light $\mathbf{s}_q(\mathbf{u})$ is expressed as

$$\mathbf{s}_q(\mathbf{u}) = \frac{1}{L}\int_{L/2}^{-L/2} d\mathbf{s} e^{iq\cdot\mathbf{u}s} = 1 - \frac{\left(\frac{L}{2}q\cdot\mathbf{u}\right)^2}{3!} + \frac{\left(\frac{L}{2}q\cdot\mathbf{u}\right)^4}{5!} - ... \quad (8)$$

$W(\mathbf{u}, \mathbf{u}')$ is the Fourier transform of the mean field potential and for pairwise interactions is written as

$$W_q(\mathbf{u}, \mathbf{u}') = 2dL^2|\mathbf{u} \times \mathbf{u}'|\mathbf{s}_q(\mathbf{u})\mathbf{s}_q(\mathbf{u}') \quad (9)$$

In integrating eq 3 over all space, the angle in $\mathbf{s}_q(\mathbf{u})$ should not be confused with that $\mathbf{s}_q(\mathbf{u}')$ nor the angle of the cross product.

This eigenvalue problem can be solved with the perturbation method by considering $\Omega_0 = -D_r R^2$ and regarding $H' = \Omega_q - \Omega_0$ as a small perturbation. The solution is conveniently expressed as spherical harmonic functions Y_{lm}. The decay in the autocorrelation function is expressed as a series in the scattering vector q. In the series expansion, the original DSO theory was limited to the two special cases of $q \to 0$ and $t \to 0$. Maeda considered solutions for more general cases,[28,29,33] and gave general expressions for both the polarized and depolarized dynamic structure factors in a form convenient for numerical computation cases.[28,29] Here, we explicitly express $g(q, t)$ as a function of the diffusion coefficients. We calculate the decay rate λ_{ql} for the lowest state corresponding to $l = 0$ at arbitrary values of q and t using second-order perturbation theory. Hence,

$$\lambda_{q0} = H'_{00} + \sum_{l\neq 0}\frac{H'_{0l}H'_{l0}}{-6D_r} \quad (10)$$

where

$$H'_{0l} = \langle Y_{00}(\mathbf{u})|H'|Y_{l0}(\mathbf{u})\rangle = \int d\mathbf{u}\, Y_{00}(\mathbf{u})[D_{\parallel}(q\cdot\mathbf{u})^2 + D_{\perp}\{q^2 - (q\cdot\mathbf{u})^2\}]\cdot\left[Y_{l0}(\mathbf{u}) + \frac{n}{4\pi}\int d\mathbf{u}' W_q(\mathbf{u}, \mathbf{u}') Y_{lm}(\mathbf{u}')\right] \quad (11)$$

To evaluate the double integrals involving cross and dot products of three vectors, one should choose either vector $\mathbf{u}'$ or $\mathbf{u}$ as the reference. The determination of H'_{00} is straightforward, whereas the determination of H'_{0l} for arbitrary l is not as simple. Fortunately, only terms up to $l = 4$ are required in order to express λ_{q0} to order q.[6] Instead of direct integration, one can also solve for λ_{q0} by applying the following relationship between the spherical harmonics:[29]

$$|\mathbf{u}\times\mathbf{u}'| = \frac{\pi}{2}\left[\frac{1}{2} - \sum_{p=2,\text{even}}^{\infty}\frac{4\pi(p-1)}{p+2}\left\{\frac{(p-3)!!}{p!!}\right\}^2\sum_m Y^*_{pm}(\mathbf{u}')Y_{pm}(\mathbf{u})\right] \quad (12)$$

where $(2n)!! = 2n\,(2n-2)...2$, $(2n-1)!! = (2n-1)\,(2n-3)...1$, and $0!! = (-1)!! = 1$.

The two approaches arrive at the same expression

$$\lambda_{q0} = D_s(1 + 2nA_2)q^2 + Bq^4 + Cq^6 \quad (13)$$

where

$$B = \frac{-2(\Delta D)^2}{135D_r} + \frac{(\Delta D)^2}{270D_r}2nA_2 - \left(\frac{1}{36}D_s + \frac{7}{2160}\Delta D\right)2nA_2L^2 - \frac{(\Delta D)^2}{4320D_r}(2nA_2)^2$$
$$= \frac{-2(\Delta D)^2}{135D_r} + \frac{(\Delta D)^2}{270D_r}2nA_2 - \left(\frac{9D_{\parallel}}{720} + \frac{11D_{\perp}}{720}\right)2nA_2L^2 - \frac{(\Delta D)^2}{4320D_r}(2nA_2)^2 \quad (14)$$

$$C = \left(\frac{3087}{2\,857\,680}D_s - \frac{1386}{8\,573\,040}\Delta D\right)\left(\frac{\Delta D}{D_r}\right)2nA_2L^2 + \left(\frac{41}{201\,600}D_s + \frac{1}{9450}\Delta D\right)2nA_2L^4 - \left(\frac{3087}{2\,2861\,440}D_s - \frac{1386}{68\,584\,320}\Delta D\right)\left(\frac{\Delta D}{D_r}\right)(2nA_2L)^2$$
$$= \left(\frac{D_{\parallel}}{5040} - \frac{D_{\perp}}{1134}\right)\left(\frac{\Delta D}{D_r}\right)2nA_2L^2 + \left(\frac{41D_{\parallel}}{201\,600} + \frac{D_{\perp}}{11\,200}\right)2nA_2L^4 - \left(\frac{D_{\parallel}}{40\,320} + \frac{D_{\perp}}{9072}\right)\left(\frac{\Delta D}{D_r}\right)(2nA_2L)^2 \quad (15)$$

$$A_2 = \frac{dL^2\pi}{4} \quad (16)$$

$$D_s = \frac{1}{3}(D_{\parallel} + 2D_{\perp}) \quad (17)$$

$$\Delta D + D_{\parallel} - D_{\perp} \quad (18)$$

Equation 13 clearly indicates that the primary relaxation mode decay rate measured in a nondilute suspension involves the thermodynamic interactions represented here with the second virial coefficient A_2, the directionally oriented translational self-diffusion coefficients $D_{\parallel}$ and $D_{\perp}$ and the rotational mobility D_r. The term linear in q^2 depends solely on the translational self-diffusion coefficient and its associated interactions, whereas the deviation from this q^2 dependence is enhanced at high q and is dependent on all of the possible mobilities and interactions. The prefactor of the q^2 term, which we call the "cooperative diffusivity" D_t, represents the rate of dissipation of osmotic pressure or concentration gradients due to molecular translational motions. The major contribution to the nonlinear terms is the translational−rotational coupling defined as $\Delta D/D_r$. It is not evident how the coefficients of the terms in q^4 and q^6 in the expression for $\lambda_{q,0}$ depend on concentration, because the concentration dependencies of the self-diffusivities ΔD and D_r are not known. It is important to realize that the concentration dependence of the decay rate is expressed in two ways. One is explicit, arising from the interaction potential W. The other is implicitly hidden in the self-diffusivities because they arise from the topological and hydrodynamic interactions.

As $q \to 0$, the leading term in eq 13 becomes

$$\lambda_{q0} = D_s(1 + 2nA_2)q^2 \quad (19)$$

as derived earlier in the DSO theory. When one probes a long length scale, intensity from the long-range motions, i.e., translation, dominates, and contributions to the spectral dynamic structure factor representing more local motions such as rotation are small. Consequently, the measured decay rate contains no contribution from the rotational diffusivity.

In a dilute suspension ($n \to 0$), the decay rate to order q^4 reduces to

$$\lambda_{q0} = D_s q^2 - \frac{2(\Delta D)^2 q^4}{135D_r} \quad (20)$$

Because intermolecular interactions vanish in this regime, the decay rate depends solely on the self-diffusivities, and includes only the influence of friction. Negative deviations (downward curvature) from linearity of the decay rate versus q^2 plot are, in this case, thus the effect of translational−rotational coupling. It is interesting to note that eq 20 is the same as that derived for the dilute rod limit by Rallison and Leal using the slender body theory of hydrodynamics.[30]

3. Experimental Section

3.1. Sample Preparation. The poly(γ-benzyl-α-L-glutamate) (PBLG) was purchased from Sigma Chemical Co. and used as received. Three molecular weight polymers were studied and their pertinent data are listed in Table 1. Contour lengths were determined from the weight-average molecular weights on the basis of total intensity light scattering experiments performed by the vendor. The monomer molecular weight is 219 g/mol, and the monomer length is 0.15 nm.[34] The polymers were suspended in a mixture of 31.8% by mass pyridine (Aldrich,

Table 1. PBLG Characterization[a]

Lot #	weight-average MW	viscosity-average MW	length
091-H-5521	100K	118K	68 nm
30-H-5515	187K	187K	128 nm
123-H-5523	248.7K	280K	170 nm

[a] The lengths are calculated from the weight-average molecular weight using 1.5 nm/monomer for the α helix.

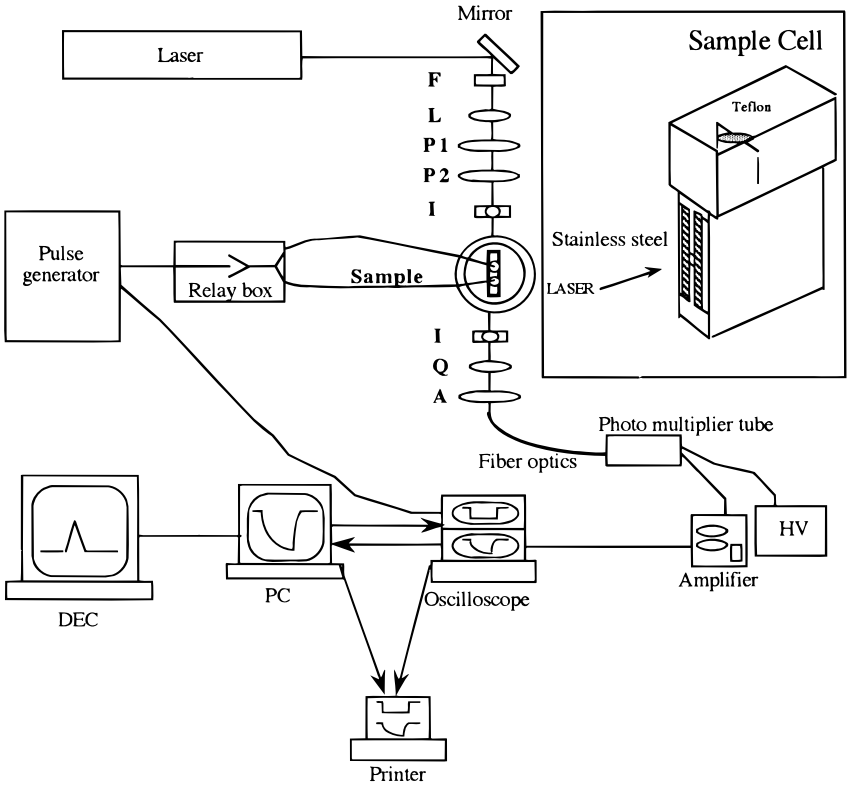

Figure 1. Schematic diagram of the transient electric birefringence apparatus. F = spatial filter, L = converging lens, I = iris, P1 = Glan laser polarizer, P2 = Glan−Thompson polarizer, Q = quarter waveplate, and A = Glan−Thompson analyzer.

HPLC grade) and 68.2% *N*,*N*-dimethylformamide (DMF) (Aldrich, HPLC grade). Both DMF and pyridine are good solvents for PBLG.[35] In these solvents, PBLG is uncharged and forms an α helix without aggregation.[31,34] The particular concentration of the solvent mixture was used previously[36] and specifically for a dynamic light scattering study of a composite liquid comprised of silica spheres and PBLG.[37] A detailed description of the cuvette cleaning procedure used in the DLS study is provided elsewhere.[34] Polymers were first dried under vacuum at room temperature for 2 days to eliminate water contamination. A clean concentrated suspension was made in two clean cuvettes. We made up the sample stock by filtering the solvent with a 0.01 μm Teflon filter (Millipore) into the first cuvette containing dried polymer. The sample was sealed and allowed to equilibrate for 2 days in the Aldrich Atmonbag containing desiccant and filled with nitrogen. We then removed dust from the polymers by filtering the solution through a 1 μm Teflon filter into the other clean cuvette. During the concentration dependence studies, the same solution was successively diluted with pure solvent mixture filtered through 0.01 μm Teflon filters. When the concentration reached approximately 10 mg polymer/mL solvent, the solution was filtered through a 0.45 μm filter. No extensive cleaning was done for the solutions in the TEB study, except that the sample cell was cleaned with toluene and ethanol before each experiment.

3.2. Dynamic Light Scattering. All of the DLS measurements were made at 25.0 ± 0.1 °C with a 514.5 nm Lexel argon laser and a Brookhaven Instruments BI200 photogoniometer. Data for the long rods were taken from suspensions in quartz rectangular cuvettes at the following 7 angles: 109.93°, 99.97°, 90°, 80.03°, 70.07°, 60.11°, and 34.87°, whereas data for short rods were taken from suspensions in cylindrical cuvettes at every 10° ranging from 30−130°. The laser power was varied from 30 to 750 mW, and data were collected between 10 min to 2.2 h, depending on the angles and sample concentrations. A Brookhaven Instruments BI6000 correlator with 522 maximum channels was used to compute the time autocorrelation of the scattered intensity. The correlation functions were analyzed by the standard program CONTIN in terms of a continuous distribution of exponential decay times.[27] The best solutions were chosen with the smoothing constraint (probability to reject) of 0.4, although very similar solutions were obtained from probability to reject of 0.2 and 0.6. The chosen distributions were reported in terms of the relaxation frequencies calculated from the intensity-weighted apparent hydrodynamic radii. The correlation functions were also analyzed using sums of exponentials. There were no significant differences between these fits and the CONTIN fits.

3.3. Transient Electric Birefringence. The birefringence apparatus used in this work is similar to that used by Elias and Eden[5] to measure moderately fast birefringence signals. A diagram of the apparatus is given in Figure 1. The light source is a Spectra-Physics model 127 (35 mW) He−Ne laser operating at $\lambda_0 = 632.5$ nm. The vertically polarized laser beam first passes through a spatial filter (F) which removes random fluctuations from the laser light intensity profile. The beam then passes through a converging lens (L), a Glan Laser polarizer (P1) of extinction ratio of 10^{-5} and a Glan−Thompson polarizer (P2) of extinction ratio 10^{-7}, both set at 45° to the beam polarization and the direction of the applied electric field. The beam diameter is reduced to 0.5 mm with a converging lens before entering the sample cell. The cell is made of a Teflon block spacing between two stainless steel electrodes and sitting in a strain-free quartz UV cuvette. The cell path length l is 20 mm and the electrode gap is 2 mm. The total sample volume is approximately 0.7 cm.^{3} Following the cell is a quarter-wave plate (Q) converting the exiting elliptical light to retarded linear polarization. Finally, the light passes through another Glan−Thompson analyzer (A) and is detected by a photomultiplier tube (Burle Supply 1P28A). The resulting voltage is then amplified by a Comlinear CLC100 amplifier and digitized by an HP-54200A digitizing oscilloscope. Assuming linear response of the system, we note that the voltage is directly proportional to the light intensity. The light intensity data $I(t)$ were transferred to a PC750 P-90 and were converted to birefringence according to[5]

$$\frac{\Delta I(t)}{I_\beta} = \frac{\sin^2\left[\beta - \frac{\pi l}{\lambda_0}\Delta n(t)\right] - \sin^2\beta}{\sin^2\beta + K_{ex}} \qquad (21)$$

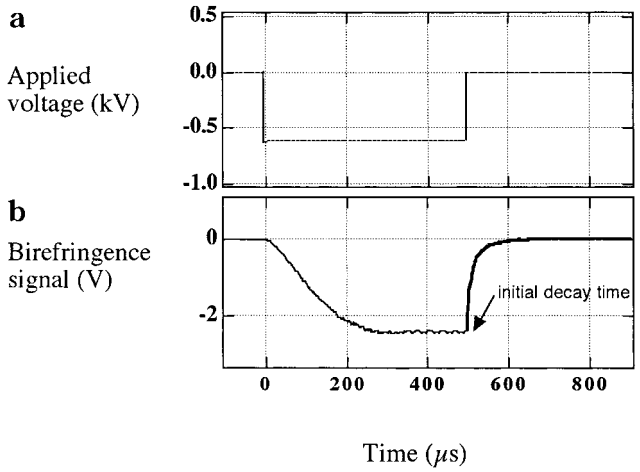

Figure 2. (a) Applied voltage (b) detected light intensity $I(t)$ from the 128 nm length PBLG solution at nL^3 =10. $I(t)$ is proportional to the birefringence $\Delta n(t)$. See eqs 21−24 of the text.

$\Delta I(t)$ is the relative change in the intensity due to the birefringence of the suspension, I_β is the nonretarded scattered light intensity, and β, the angle between the analyzer and its crossed position, is adjusted during the experiment to achieve the optimal signal-to-noise ratio. $\Delta n(t)$ is the temporal change in the sample birefringence and K_{ex} is the extinction ratio of the complete system, which is 10^{-5} in our apparatus. Throughout the study, a single negative square wave electric pulse with 30 ns rise time and 20 ns fall time was introduced to the sample at the rate of 1 Hz by a Velonex 360 pulse generator requiring an external impedance of 200 Ω. A typical pulse width ranges from 300 to 500 μs, and the electric field varies from 1 to 4 kV/cm. Data taken at room temperature were averaged over 300 pulses per run, and each data point reported in this paper resulted from 7 to 10 runs. An example of the applied voltage and the corresponding birefringence signal are illustrated in Figure 2. The characteristic coefficient D_r can be determined from the rising signal after the field is turned on or the decaying signal after the field is turned off. Here, we analyze only the latter because it requires no knowledge of the permanent and induced dipole moments of the PBLG. The following equation describes the time-dependent birefringence decay of monodisperse cylindrical particles

$$\Delta n(t) = \Delta n_0 \exp(-6D_r t) \tag{22}$$

where Δn_0 is the steady-state amplitude of the birefringence at a particular field strength, and $(6D_r)^{-1}$ is the relaxation time. The time t starts when the field is turned off. Notice that if $\beta = 0$, eq 21 can be approximated to provide D_r directly according to

$$I(t) \approx I(0) \exp(-12D_r t) \tag{23}$$

When β is smaller than 10° but much larger than half of the steady-state retardation [proportional to the saturated birefringence Δn_s and the orientational distribution, which depends on the permanent dipole moment (μ) and polarizability (α) of the molecules], the intensity will be directly proportional to the birefringence

$$I(t) \approx I(0) \exp(-6D_r t) \tag{24}$$

Rotational diffusion coefficients were obtained from CONTIN using the same input parameters mentioned in the previous section.

It is important to realize that the birefringence decay measured by TEB, which provides the same information as the forward-angle depolarized DLS measurement, depends on the collective reorientation time.[38] In principle, it includes static and dynamic orientational correlations between molecules. However, in the comparisons of DE theory and the experimental data, it has usually been assumed that the measured quantity is the single molecule rotational diffusion coefficient, mainly because the effect of the correlation is not exactly known and is usually assumed to be relatively small.[6,18] However, Maeda[29] has shown that within the DSO theory, the single molecule rotational diffusion coefficient is related to the measured (collective) rotational diffusion coefficient by

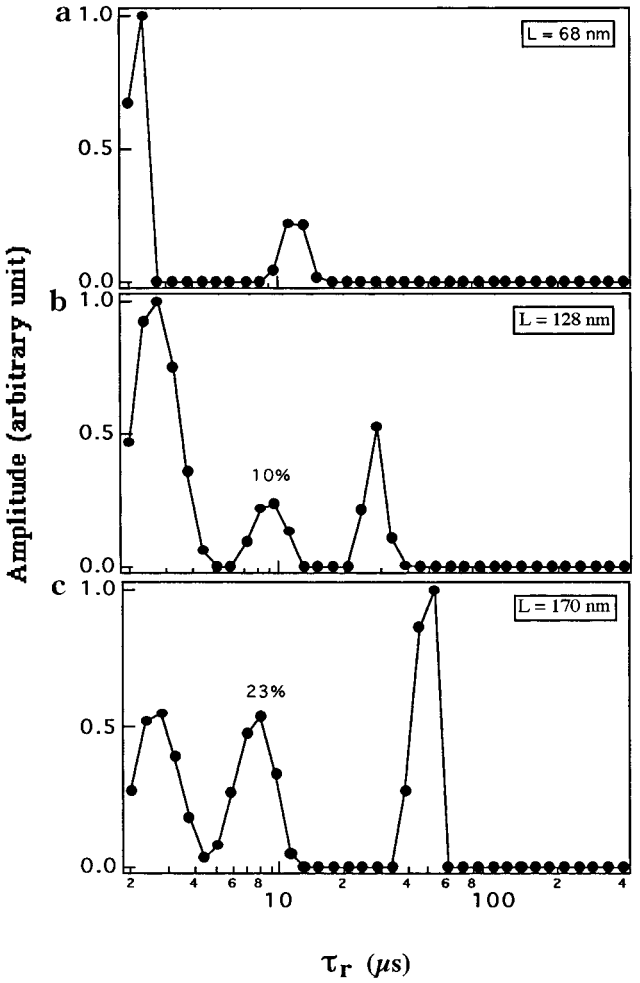

Figure 3. Relaxation time distribution from CONTIN analysis of dilute suspensions of (a) 68 nm at $nL^3 = 5.5$, (b) 128 nm at $nL^3 = 6.0$, (c) 170 nm at $nL^3 = 6.0$.

$$D_r(\text{single}) = D_r(\text{collective}) / \left(1 - \frac{n}{n^*}\right) \tag{25}$$

where $n^* = 16/\pi d L^2$, the Onsager critical concentration. Equation 25 predicts that the measured rotational diffusion coefficient goes to zero at n^*.

4. Results and Discussion

4.1. Rotation. In Figure 3, we illustrate CONTIN analysis of the birefringence decay times τ_r, defined as $1/(6D_r)$, from suspensions of three different rod sizes at similar concentrations, 5−6 rods/L^3. CONTIN resolves two decay times for the shortest rod (L = 68 nm), and three relaxation times for the longer ones (L = 128 and 170 nm). The fastest relaxation time does not contribute much and is most likely an artifact. Its amplitude and value vary with data set and depend on the input parameters to the CONTIN analysis. This artifact has consistently been observed in previous work.[34,39−41] In any case, its contribution is very small, and we do not discuss it further. The slowest relaxation time is due to

Table 2. Comparison of the Experimentally Measured Rotational Relaxation Times of PBLG in Infinitely Dilute Solutions with the Broersma Predictions for Rigid Rods[a]

rod length (nm)	Broersma prediction (μs) (d = 1.5 nm)	Broersma prediction (μs) (d = 2.2 nm)	experimental measurements (μs)
68	3.5	4.1	12.0 ± 2.0
128	17.8	20.5	27.6 ± 3.0
170	37.1	43.3	40.0 ± 2.0

[a] The infinite dilution values are from extrapolation of the experimental values in the dilute regime.

rotation and agrees well with the Broersma theoretical equation for rigid rods:[42]

$$D_r = \frac{3k_BT}{\pi\eta_s L^3}(\varphi - \xi) \tag{26}$$

where

$$\varphi = \ln\left(\frac{2L}{d}\right)$$

$$\xi = 1.14 + 0.2\varphi^{-1} + 16\varphi^{-2} - 63\varphi^{-3} + 62\varphi^{-4}$$

and η_s is the solvent viscosity (0.8221 cP). Table 2 compares the average experimental diffusion coefficient for the rotational process with the calculations of the rigid rod model. Rotational diffusion coefficients at infinite dilution (D_{ro}) are obtained from extrapolating D_r to $nL^3 = 0.001$. Because we calculate rod lengths from polymer molecular weights reported by the vendor, the discrepancy between experimental and predicted decay times, particularly for the shortest rod, is possibly due to inaccuracy in the molecular weight. Polydispersity is another factor that could lead to some discrepancy.

In Figure 4, we illustrate CONTIN analysis of the birefringence decay times τ_r, from suspensions of the three different rod sizes at higher concentrations. In the top panel of Figure 5, we summarize our results for the overall rotational relaxation times over the entire concentration range studied. The middle graph of Figure 5 compares our experimental values of the normalized rotational diffusion coefficients (D_r/D_{ro}) to the simulation results of Bitsanis et al.[22,23] the modified caging theory of Keep and Pecora,[18] and the theoretical results of Fixman.[20,21] On the bottom graph in Figure 5, we show, in addition to the measured time, the single molecule rotational relaxation time as corrected by Maeda's formula, eq 25. The correction is significant at the highest concentrations studied.

In addition to the rotational process, a faster relaxation at about 8 μs is detected from the rods having contour lengths of 128 and 170 nm. For the 128 nm long rod, this decay process is observed in only 12 of the total experimental runs and contributes to at most 10% of the decay amplitude. This process makes a larger and more consistent contribution in a dilute suspension of the 170 nm long rod. Because this fast decay becomes more important for the longer rod, we believe that it represents the first internal bending mode and is an indication of the flexibility of our long PBLG.

Although PBLGs exhibit some flexibility, they are still highly stiff without any apparent higher order internal motions. Undoubtedly, among the synthetic polymers, they offer one of the best models to elucidate the dynamics of rodlike particles. As a consequence, we analyze the slowest decay mode based on the theories

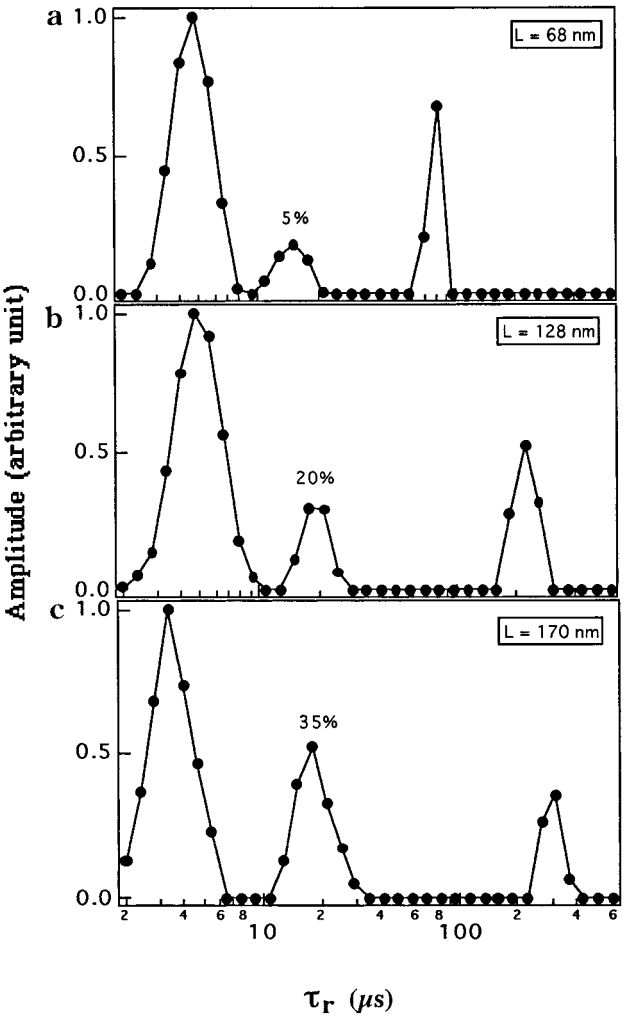

Figure 4. Relaxation time distribution from CONTIN analysis of concentrated suspensions of (a) 68 nm at $nL^3 = 119.6$, (b) 128 nm at $nL^3 = 135.3$, (c) 170 nm at $nL^3 = 120.2$.

for rotation of rigid polymers and ignore the bending motion and its coupling with rotation. The top graph of Figure 5 shows the decay time of the slowest process as a function of the rod crowding. The dashed lines are simply to guide the eye. Above 100 rods/L^3, rotations of the two longest rods clearly become faster than expected from the theory of rigid rod rotation in nondilute solutions (bottom part of Figure 5). This is probably an indication of flexibility.

The Keep and Pecora model of a rod confined to a cage is thought to be valid above $nL^3 > 50$, where caging is expected to be complete. In this modified version of DE theory, the molecule must travel a distance f, a fixed fraction of the rod length, in order for a new cage to manifest. We find $f = {}^1/_8$ provides the best fit to our experimental data at $80 < nL^3 < 120$. This value is within the range ${}^1/_{1.5} < f < {}^1/_{8.7}$ observed in previous studies.[18] Between 50 and 80 rods/L^3, f seems to increase with concentration, suggesting that it is a concentration-dependent quantity.

The estimation of the cage sizes, their concentration dependence in the DE theory, and the modifications of the DE theory have been questioned. The argument rests on the equilibrium conditions of the undistorted cage.[20,23] The model of Fixman,[21] on the other hand, explains the rotational dynamics in term of the rapid dissipation of the caging forces. Initially, a slight rota-

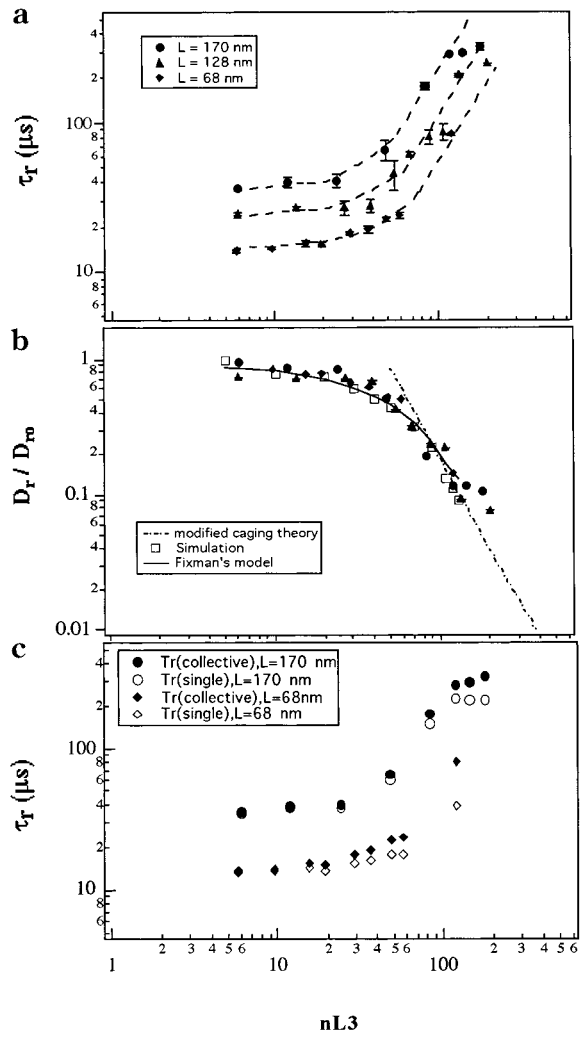

Figure 5. Rotational relaxation time and normalized rotational diffusion coefficient plotted against polymer concentration. In the middle graph, the experimental data are compared with the results from Brownian dynamics simulation, a modified caging theory, and the Fixman theory. In the bottom graph, the experimental data are compared with the single molecule values calculated from eq 25.

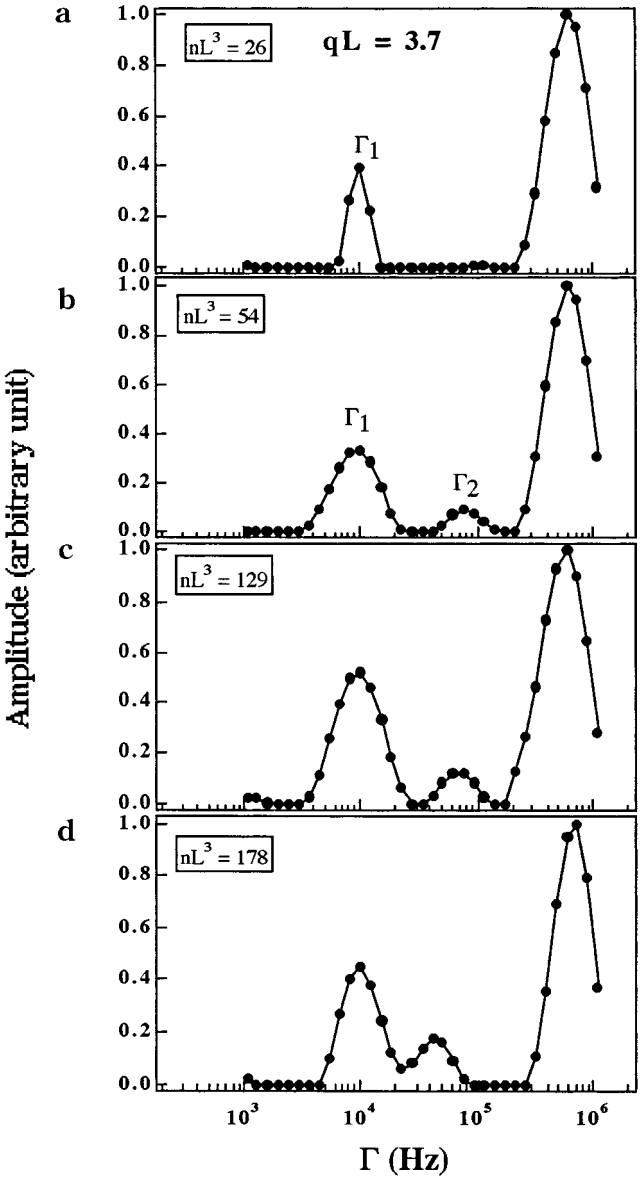

Figure 6. Distribution of dynamic decay rates obtained from CONTIN analysis of DLS experiments on 128 nm long rods. qL is held constant at 3.7.

tion of a probe disturbs the equilibrium and produces a free energy stored in the neighborhood of the probe. The stored free energy is released by two mechanisms: a very fast mechanism of slight rotation of the neighbor and a slow mechanism of DE longitudinal diffusion.

In Figure 5, data from the Fixman model, which are available up to nL^3 of about 150[23] are compared favorably with our experimental results, the modified caging theory,[18] and the Brownian dynamics simulation.[23] At higher concentrations, an extrapolation of the Fixman model differs from the simulation but agrees better with the experimental data. Although the former is believed to originate from an overestimation of the short-time rotations,[23] the latter may simply be fortuitous because the discrepancy between the experimental data and simulations is more likely due to flexibility.

Because one goal of our investigation in this section is to obtain the absolute D_r at a particular suspension concentration to use in a further investigation of the DLS spectrum, we utilize the comparison of our TEB results to the theoretical predictions. In the following analysis of the DLS results, we use the D_r from the Fixman model fits to the TEB data presented in Figure 5 at concentrations up to 100 rods/L^3 in the DSO expression for the light scattering main mode in order to extract the translational diffusivities. At higher concentrations, D_r is calculated according to the modified caging theory of Keep and Pecora with $f = 1/8$.

4.2. Cooperative Translation. In this section, we discuss the DLS spectra of solutions of rods of two lengths:

PBLG of length 68 and 128 nm. Figure 6 represents the DLS spectrum obtained from CONTIN analysis of the 128 nm long rod suspensions at a fixed scattering wave vector $q = 2.89 \times 10^7$ m^{-1}. Data from the 68 nm long rods demonstrate similar behavior. The abscissa shows the distribution of the characteristic decay constant or frequency Γ, equivalent to the inverse decay time $1/\tau$, in the dynamic structure factor. The decay rate corresponding to the largest Γ is likely due to an artifact because its location varies with the input parameters to the CONTIN analysis. Up to the concentration of about 40 rods/L^3, only one dynamic process (with its peak at Γ_1) is observed. At a higher concentration, a

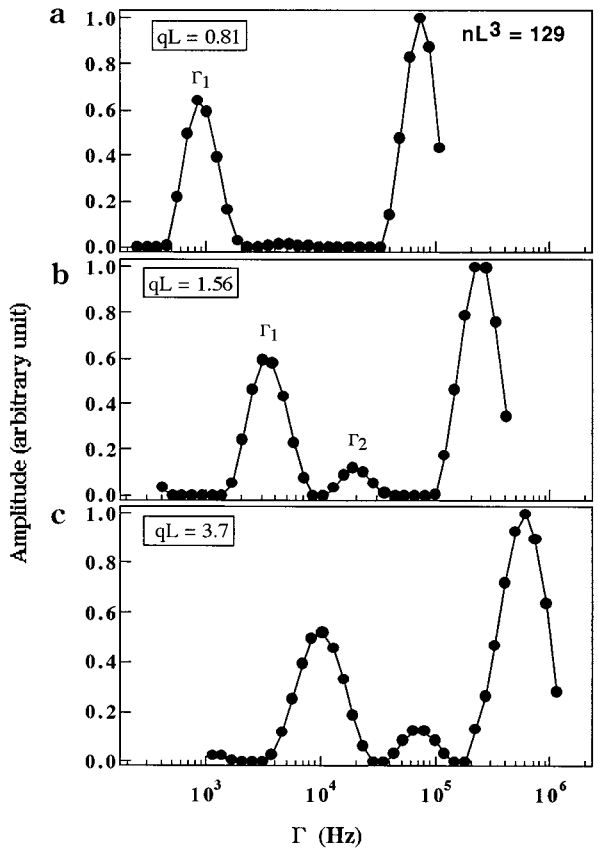

Figure 7. Distribution of decay rates obtained from CONTIN analysis of the DLS time correlation functions of the 128 nm long rods. The rod concentration is held constant at $nL^3 = 129$.

faster decay process (with its peak at Γ_2) appears. Although this fast process becomes more important with increasing polymer concentration, its decay rate becomes slower. This behavior is observed at all interaction length scales ($1/q$). On the other hand, the behavior of the slow process varies with the interaction length scale. At low q, the relaxation is slightly faster with higher concentration, whereas, at high q such as the one shown in Figure 6, the concentration dependence of this slow process cannot be determined accurately. A detailed discussion of the angular dependence of this dynamic process is given below in connection with Figure 9. In Figure 7, we demonstrate the CONTIN output from a 128 nm long rod suspension at a fixed concentration at different scattering vector lengths. Although the fast process Γ_2 is not observable at low q, it is clearly detected at q above 1.22×10^7 m^{-1}. The fact that the fast-mode amplitude increases with increasing angle and decays more slowly as concentration increases indicates a strong influence of rotation. Hence, it is likely that this mode arises from both rotation and translation (and likely also contains effects of the translational−rotational coupling). The anisotropic translation giving rise to the dependence of the rate of translation in a given direction on the instantaneous polymer orientation results in the translational−rotational coupling. In the qL range we are interested in, previous theories predict two decay rates for long thin rods in dilute and semidilute concentrations.[17,29,30] For example, Rallison and Leal express the light scattering spectrum as a sum of the two exponentials in time, both of which involve the two dynamic processes.[30] One term is dominated by the translational diffusion coefficient, whereas the other is dominated by the

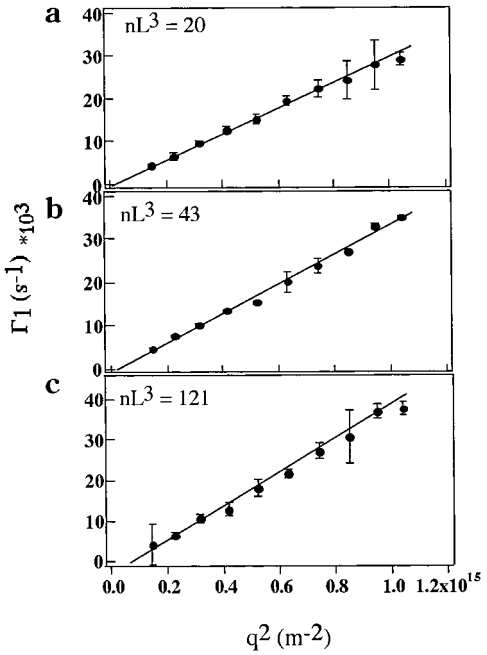

Figure 8. Decay rates of the dominant DLS mode for the 68 nm long rod as a functions of q^2 for three concentrations.

rotational diffusion coefficient. A similar peak believed to be the dynamic mode dominated by rotation is also observed in other rodlike[17,34] systems and is currently under detailed investigation.[43]

A very weak fourth peak at small Γ is often seen at a large q and high nL^3, and its position varies with the definition of the CONTIN sampling window. Because of its low intensity and erratic position, this peak possibly is related to the slow mode seen in many other systems of both rodlike and flexible polymers.[26]

We focus only on the angular and concentration dependence of the dominant peak Γ_1. In Figure 8, we plot Γ_1 versus q^2 measured from the suspensions of the 68 nm long rods. The frequency Γ_1 scales with q^2 so it is purely due to the mutual translational relaxation. Russo et al.[31] and DeLong and Russo[26] observed, from cumulant analysis, a positive deviation from linearity at $q^2 > 0.4 \times 10^{-15}$ m^{-2} in dilute suspensions of PBLG with lengths ranging from approximately 0.3 times shorter to 1.6 times longer than those in this study. The upward curvature from the suspensions of long rods was attributed to the enhancement of rotation at high qL according to the existing theories,[32,44−47] whereas the deviation for short rods resulted from intramolecular interference of polydisperse samples. However, a linear relationship was expected for monodisperse short rods.

Our results for a dilute suspension of the 128 nm long rods are plotted in a similar way in Figure 9. Again, no positive deviations from q^2 are observed at low concentrations. The results at higher concentrations, on the other hand, show negative deviations at high q. The latter feature was also observed in the cumulant analysis[26] and was explained according to the DSO theory[24] and the Maeda reformulation of the DSO theory.[29] Briefly, the shift from positive to negative deviation indicated that the dynamic properties measured by DLS at high qL were not subjected to the long-range driving forces affecting the dynamic properties measured at low qL. The negative deviation increased as concentration increased. This concentration dependence was attributed to (i) more restricted rotational

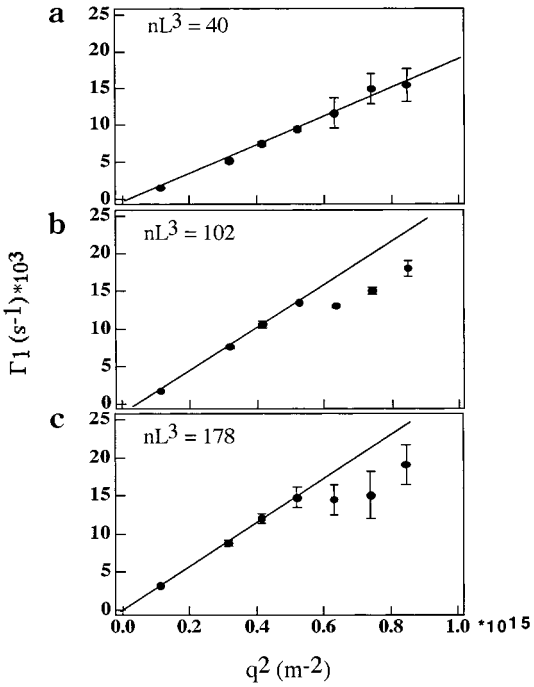

Figure 9. Decay rates of the dominant DLS mode for the 128 nm long rod as functions of q^2 for three different concentrations.

motion which diminished the positive deviation and (ii) increasing particle concentration which contributed to a larger negative deviation.

The interpretation of the results measured at an intermediate time in this work has similarities to and important differences from the cumulant analysis. According to eq 13, the term linear in q^2 is the translational diffusivity, expressed in terms of the self-diffusion coefficient and the thermodynamic second virial coefficient. In the dilute regime, our calculation predicts a negative deviation, instead of a positive curvature as in the cumulant analysis. As can be seen from eq 14 if we approximate n to be very small, the nonlinearity results from the $-2(\Delta D)^2/135D_r$ term. This nonlinearity is not observed experimentally because of the small $(\Delta D)^2/D_r$ value in the dilute regime for the rods studied. Physically, no coupling is detected because of the weak translational anisotropy of the rather short rods and the fact that rotational relaxation is faster than translation.

At higher concentrations, deviations from linearity take place due to the combined effects of the translation, the rotation, and the translational anisotropy. At small interacting length scales, the factor B consisting of three negative terms and one smaller positive term is responsible for the nonlinearity. At even smaller length scales, terms in the factor C will become more influential. When the absolute values of the first two terms described in eq 15 become greater than the last one, the Γ_1 versus q^2 curve starts to bend upward. Indeed, this is what we observe at $q^2 > 0.7 \times 10^{15}$ m.$^{-2}$ On the other hand, at a high-enough concentration when the last term dominates, the negative deviation prevails. For a very long rod, nonlinearity should be easily detected in both the dilute and semidilute regimes because of a slower rotation and a larger translational anisotropy. The effects of this anisotropy are also enhanced with larger L.

We now extract mutual translational diffusivities and self-diffusivities in the parallel and perpendicular directions from the DLS spectrum with our analytical expressions eqs 14, 17, and 18. In Figure 10, we plot the slopes from Figures 8 and 9 as a function of polymer concentration. The cooperative diffusivity D_t, defined as the coefficient of the q^2 term in eq 13, is the mutual diffusion coefficient. The transitions from the dilute to semidilute regimes at $nL^3 = 29$ and 40 for the 68 and 128 nm rods, respectively, are the same as the transitions seen from our TEB data. These concentrations are also close to those found previously, where for similar molecular weights 100K and 187K, nL^3 of 15−20 and 21−60 were reported.[17,26,31,34]

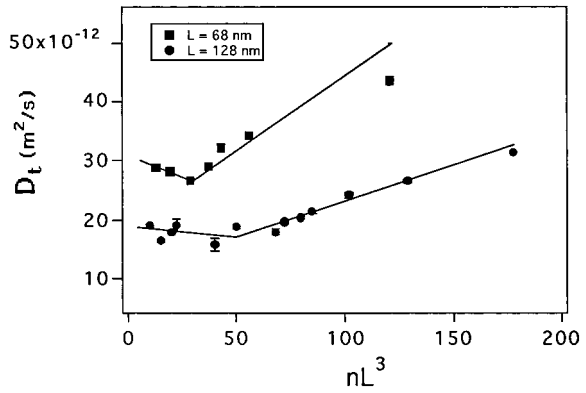

Figure 10. Mutual diffusion coefficients of two different rod sizes as functions of polymer concentration.

The dependence of the mutual diffusion coefficient on concentration in each regime represents the competition between osmotic pressure enhancing the observed diffusion and hydrodynamic friction retarding the motion.[31] The diffusion virial coefficient k_D is the result of the two effects according to

$$D = D_0(1 + k_D c) \tag{27}$$

$$k_D = 2MA_{2(ZOS)} - k_f - v \tag{28}$$

where v is the specific volume and $A_{2(ZOS)}$ is the hard rod second virial coefficient introduced by Zimm, Onsager, and Schulz for $L \gg d$[48] as

$$A_{2(ZOS)} = \frac{\pi N_A d L^2}{4M^2} \tag{29}$$

N_A is Avogadro's number and M is the polymer molecular weight in Da. The experimental D_o is determined from the intercept of the linear fit in each regime as shown in Figure 10 and is compared to the theoretical prediction of Broersma[42] for $L/d > 5$ to obtain a geometric diameter d.

$$D_o = \frac{k_B T}{3\pi\eta_s L}\left[\varphi - \frac{1}{2}(\gamma_{\parallel} + \gamma_{\perp})\right] \tag{30}$$

where

$$\varphi = \ln\left(\frac{2L}{d}\right)$$

$$\gamma_{\parallel} = 0.807 + 0.15\varphi^{-1} + 13.5\varphi^{-2} - 37\varphi^{-3} + 22\varphi^{-4}$$

$$\gamma_{\perp} = -0.1937 + 0.15\varphi^{-1} + 8.1\varphi^{-2} - 18\varphi^{-3} + 9\varphi^{-4}$$

The slope k_D, the $A_{2(ZOS)}$ calculated from the geometric d of 1.8 ± 0.4 nm, and the specific volume of 0.791 cm^3/g

Table 3. Comparison of the Results from the Linear Fits to D_t vs c in Two Concentration Regimes with the Theoretical Predictions

	68 nm long rods		128 nm long rods	
	dilute regime	semidilute regime	dilute regime	semidilute regime
$D_o \times 10^{11}$ (m^2/s)	3.05 ± 0.04	1.87 ± 0.23	1.90 ± 0.10	0.90 ± 0.20
exptl k_D (cm^3/g)	−8.59 ± 1.13	14.5 ± 5.67	−7.12 ± 3.01	33.82 ± 4.11
Peterson k_D (cm^3/g)	−27.76 ± 5.85	na	−0.26 ± 8.21	na
Itou et al. k_D (cm^3/g)	−16.39 ± 5.09	na	−0.37 ± 7.97	na
exptl k_f (cm^3/g)	73.42 ± 1.13	50.32 ± 5.67	137.83 ± 10.54	104.18 ± 8.78
Peterson k_f (cm^3/g)	92.59 ± 5.81	na	148.14 ± 8.72	na
Itou et al. k_f (cm^3/g)	81.21 ± 5.10	na	148.03 ± 8.52	na

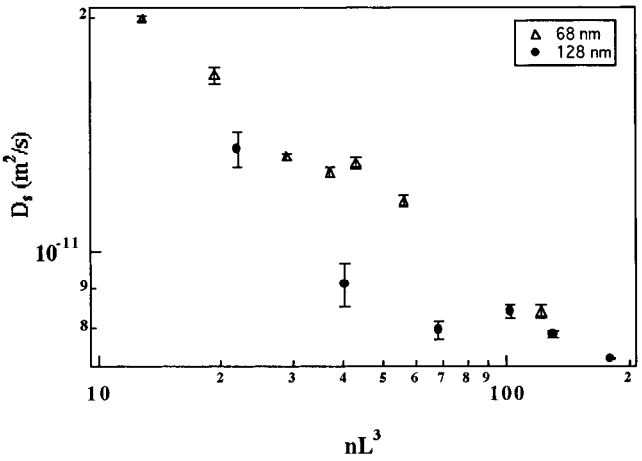

Figure 11. Self-translational diffusion coefficients of the 128 nm long rod as obtained from eq 13 as a function of concentration.

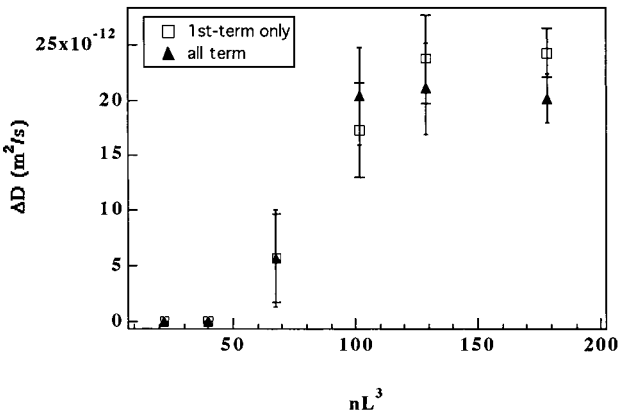

Figure 12. Translational anisotropy calculated from eq 14 and experimental values of B and D_s.

for PBLG are then used to calculate the experimental k_f values. Theoretical k_f values for dilute suspensions due to Peterson[49] and Itou et al.[50] are also reported in Table 3:

$$\text{Peterson: } k_f = \left(\frac{RT}{3\eta_s}\right)\left(\frac{L^2}{D_o M}\right)\left(\frac{3d}{8L}\right)^{2/3} \tag{31}$$

$$\text{Itou: } k_f = \left(\frac{k_B T}{3\eta_s}\right)\left(\frac{3A_{2(ZOS)}N_A^{1/2}}{2\pi}\right)^{2/3}\left(\frac{M^{1/3}}{D_o}\right) \tag{32}$$

The theoretical value of k_D is calculated from the theoretical k_f by using the diameter 1.8 ± 0.4 nm.

The D_o from the dilute regime of the two systems provide the geometric diameters 1.5 and 1.8 nm, in good agreement with those in the literature.[13,31,34,51] The intercepts from the semidilute regime give unreasonably large diameters,[50] indicating the need to measure diffusion in the dilute regime as reported in an earlier work.[34] The experimental k_f and k_D for both rods are in reasonable agreement with the theoretical values. Tracy and Pecora studied 102K PBLG suspended in DMF only and reported a similar k_D value of −4 ± 4 cm^3/g.[34] The k_D in the second regime of the short rod identifies very well with 14 ± 1 cm^3/g in the previous work. The k_D for the long rod is about twice the value for the short one. This finding is supported by eqs 28, 29, and 31, where k_D is roughly proportional to L.

4.3. Self-Translation. The self-diffusion coefficient D_s can be extracted according to eq 13 simply from the cooperative diffusivity D_t, $D_s = D_t/(1 + 2nA_2)$. As expected,[22,23,26,31,51,52] the self-diffusion coefficient D_s diverges from the mutual one (Figure 11). The self values of the short rods are the same order of magnitude as those measured directly on an 103K-labeled PBLG using DLS and the fluorescence photobleaching recovery technique.[51] The direct measurements exhibited three regimes with a strong decrease at $40 < nL^3 < 200$ between two regimes of relatively constant D_s. Although the onset of the decreasing zone in this direct study agrees favorably with the transitions in our D_t and D_r data, Figure 11 does not clearly show three regimes. This is probably due to the definitions of the friction coefficients for the mutual and self-translations in the mean field theory. The mean field approach of Doi, Shimada, and Okano[24] assumes that the friction coefficient for mutual diffusion is the same as that for self-diffusion. Bu et al.[51] argue from their experiments that these friction coefficients are different. This observation suggests a weak point in the DSO theory and reveals a possible limitation of extracting D_s from the DLS D_t. More experimental data comparing self- and mutual-diffusion coefficients are needed to give definitive answers to this question.

4.4. Translational Anisotropy. The translational anisotropy ΔD for the 128 nm long rod is found from the experimental B value at $q^2 = 7.2 \times 10^{14}$ m^{-2} by using eq 13 and eq 14. Figure 12 shows a rapid increase in ΔD at $40 < nL^3 < 100$ before it reaches a plateau at a value close to $D_{||,0}$, which is 2.4 ± 0.2 × 10^{-11} m^2/s for a diameter of 1.8 ± 0.3 nm according to Broersma's prediction[42] with $\gamma_{||}$ given in eq 29:

$$D_{||0} = \frac{k_B T}{2\pi\eta_s L}(\varphi - \gamma_{||}) \tag{33}$$

Experimentally, the anisotropy in the dilute regime ($nL^3 < 40$) is not observable; however, theoretically, it equals $D_{||,0} - D_{\perp,0}$. Using

$$D_{\perp,0} = \frac{k_B T}{4\pi\eta_s L}(\varphi - \gamma_{\perp}) \tag{34}$$

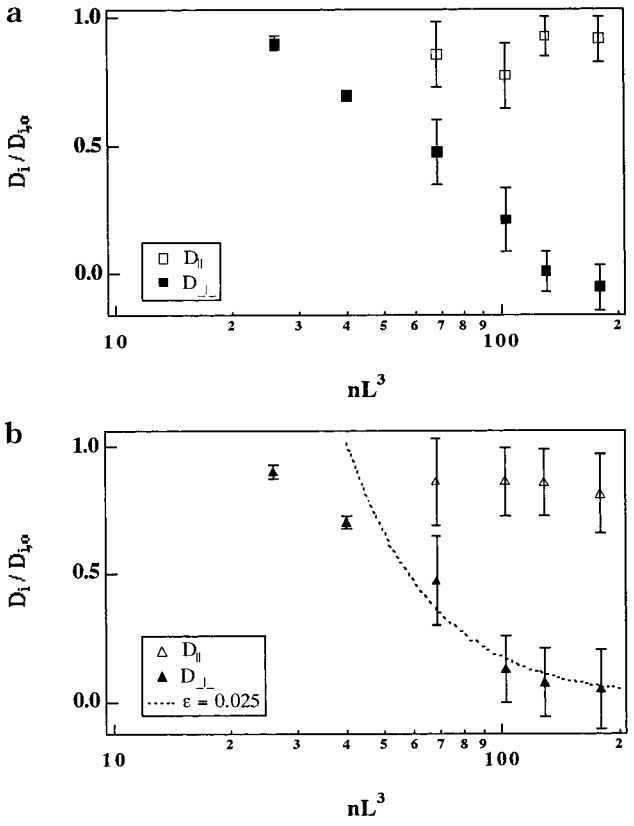

Figure 13. Self-diffusion coefficients of the translation in the directions parallel and perpendicular to the long rod axis as calculated from the experimentally obtained ΔD and D_s according to eqs 17 and 18. (a) Only the first term in eq 14 is used to obtain ΔD. (b) ΔD calculated from the experimental B using all of the terms in eq 14.

with $\gamma_\perp$ given in eq 30, we find $D_{\perp,0} = 7.7 \pm 0.3 \times 10^{-12}$ m^2/s. The larger anisotropy at a higher concentration indicates a more significant translational−rotational coupling as predicted previously.[18] We also learn from this plot that at this particular q and L, the first term in eq 14 represents the prefactor B very well. With knowledge of $D_s(n)$ and $\Delta D(n)$, we then plot the perpendicular and parallel translational diffusivities in Figure 13. It is apparent from this plot that the increment in the anisotropy is mainly due to the reduction in the transverse translation. The plateau in the anisotropy plot results from a cessation of transverse translation while the longitudinal translation remains relatively constant. Comparison to computer simulations and available theories shows qualitative but not perfect agreement.

The corrected D_r obtained from the Maeda formula eq 25 and used to calculate ΔD gives ΔD values that, even at the highest concentrations studied, are less than 10% different from those calculated from the measured D_r.

Bitsanis et al.[22,23] performed Brownian dynamics on rods of aspect ratio 50 in order to selectively elucidate the effect of intermolecular forces on each of the mobilities. Hydrodynamic interactions on a molecule and between different molecules were neglected. The result showed a modest decrease in the parallel translation to 80% of its infinitely dilute value at $nL^3 = 50$. This is in excellent agreement with our observation; however, a large discrepancy is seen in the transverse translation. The simulation shows a much sharper decrease with concentration than our experiments. Although our data reveal only a 50% reduction at $nL^3 = 50$, the simulation result diminished as much as 80%, a reduction only attained when nL^3 reaches 100 in our experiments. The dynamic mean field theory with neglect of rotational mobility surprisingly predicted an even faster reduction[12,53] $(D_\perp/D_{\perp,0}) = 0.02$ at $nL^3 = 50$.

A theory employing Green's function/perturbation approaches exists for the translation in the two directions.[54−56] Teraoka and Hayakawa[55] arrived at the following expression for the loss of perpendicular translation.

$$D_\perp = D_{\perp,o}(1 + \epsilon nL^3)^{-2} \tag{35}$$

Sato and Teramoto[56] offered an expression for the concentration-dependent parallel translation:

$$D_{||} = D_{||,0}\left(1 - \frac{ndL^2}{\rho}\right)^2 \tag{36}$$

where ϵ and ρ are dimensionless parameters. The parameter ρ is related to the mean lifetime τ of the test-rod barrier (other rods) on the test-rod path and is defined in the relation $\tau = \rho L^2/D_{||}$. The parameter ϵ depends on the geometry of the tube model similarly to the β in the original caging theory in which $D_r/D_{ro} = \beta(nL^3)^{-2}$.[3,4] Although ϵ is not known, ρ was estimated to be 13 ± 2 from zero-shear viscosity experiments on aqueous solutions of two helical polysaccharides: xanthan gum[56] and schizophyllan.[57] The best fit to our $D_\perp$ obtained at high concentration as illustrated in Figure 13b yields an ϵ value of 0.025 ± 0.01. The $D_{||}$ data subjected to a constraint 1.0 at zero concentration (Figure 14) yields $\rho = 17.3 \pm 2.0$, which is within the range of the earlier estimates.

The total self-translational coefficient can be calculated from the weighted sum of $D_{||}$ and $D_\perp$. Bu et al.[51] did not find a good match at low and high concentrations between their self-diffusivity D_s measured from fluorescence-tagged PBLG in pyridine and the sum of eq 35 and eq 36 for D_s

$$\frac{D_s}{D_{s,o}} = \frac{1}{3}(D_{||} + 2D_\perp)$$
$$= \frac{1}{2}\left[\left(1 - \vartheta\frac{n}{n^*}\right)^2 + \left(1 + \psi\frac{n}{n^*}\right)^{-2}\right] \tag{37}$$

where $\theta = 16\pi/\epsilon$, $\psi = 16\epsilon/\pi d$, and n^* is the Onsager critical concentration. However, the same formula with adjustable offsets for the baseline and the concentration captured their $D_s(n)$ in the second regime better than eq 37 did. Our method, on the other hand, gives a reasonably good fit to eq 37 as shown in Figure 14b. Extrapolation from the best fit to $n/n^* \to 1$, however, gives $D_s/D_{s,o} = 0.26$, a rather high value for a point at which the mobilities are expected to be very small.

4.5. Internal Bending. As mentioned in Section 4.1, we believe that the fastest dynamic relaxation time (excluding the very fast "artifact") observed in the TEB experiments from the 128 and 170 nm long rod suspensions is the first internal bending mode indicating the rod flexibility. Our analysis is based on a previous investigation of a flexible DNA.[39] Lewis et al.[39] reported the first internal decay time at 2.3 μs for 367 base pair (bp) DNA (approximately 135 nm contour length), with increasing values for longer DNA. They also observed, from the same DNA, an augmented decay amplitude

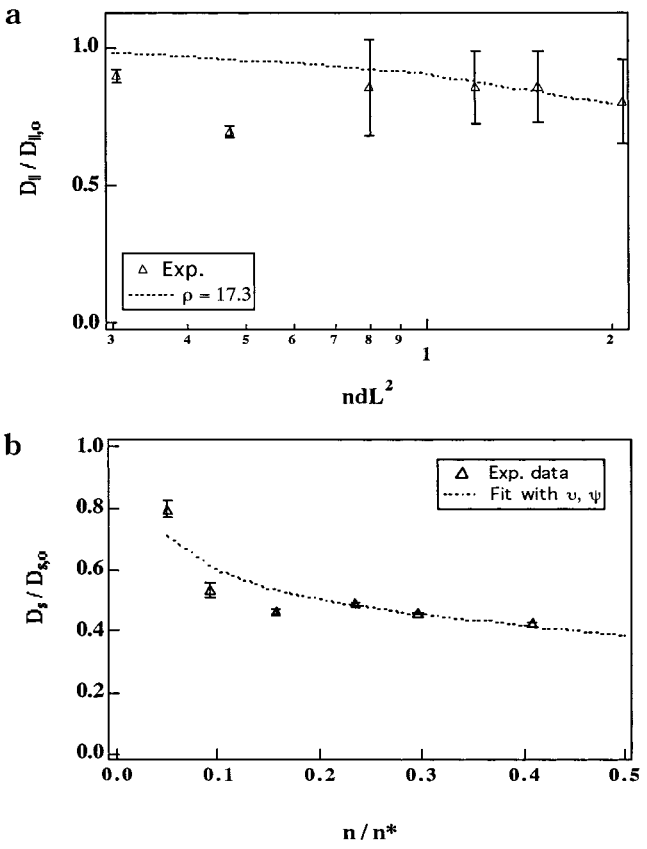

Figure 14. (a) Best comparison of the experimentally determined $D_{\|}$ to the theoretical prediction (eq 36) with α equal to 17.3. (b) Measured self-diffusion coefficient compared with two expressions. The dotted line represents $D_s = {}^1/_3 (D_{\|} + 2D_{\perp})$ or eq 36 with no adjustable offsets, and $\upsilon = 2.91$ and $\psi = 10.86$. The dashed line represents eq 36 with adjustable offsets: $b = -0.72$, $\upsilon = 1.917$, $n^+/n^* = 0.63$, and $\psi = 0.70$.

with increased electric pulse duration. We do not observe any length dependence in our dilute 128 and 170 nm long rod suspensions. One likely explanation is that the position of the internal mode is influenced by the position of the artifact peak when the two peaks are not well-separated. Moreover, the polymer lengths are not different enough to provide accurate data to elucidate the length dependence of the internal bending process. Neither do our data show any dependence on the applied pulse duration. This is probably because the birefringence corresponding to the internal relaxation is already saturated at 300 μs, the minimum pulse duration applied in our experiments, compared with the 5 μs pulses used in the study of DNA.

We follow the decay time of the internal bending as the concentration of the suspension increases. Figure 4 exemplifies the decay time distribution from concentrated suspensions of the three systems. For the two long rods, the bending relaxation is slower and more significant at increasing suspension concentrations. At 121 rods/L^3 of the shortest rods, the peak of the bending relaxation becomes detectable. Hence, even our shortest rod is not perfectly rigid. We do not observe this peak in the dilute suspension possibly because the relaxation time in the dilute suspension is too close to the artifact peak for CONTIN to resolve.

The stiffness of PBLG can be determined from its persistence length P. Unfortunately, difficulties in determining reliable values of P remain because of a lack of samples with contour lengths much larger than the expected persistence length. Consequently, the reported P value varies from 60 to 160 nm.[26,44,58] Within this window of P, the dimension of our longest rod ranges from 1 to 3 persistence lengths, indicating a rather semistiff molecule. A useful model of a semistiff molecule is the trumbell model of Roitman and Zimm who represented the polymer by three beads connected by two rigid bonds.[59] The bending strength of the bonds can be measured by a stiffness parameter which is proportional to the ratio of the decay time in the rotation to that in the bending motion. The result from the 170 nm rod, as shown in Figure 3, gives a ratio of decay times around 6.3, corresponding to the stiffness parameter about 1.0. This value suggests that the 170 nm long PBLG exhibits similar flexibility to the 367 bp DNA studied by Lewis et al.[39]

5. Conclusion

We have studied the translational and rotational dynamics of three lengths of PBLG over a wide range of solution concentrations. We have, in addition, extended the dynamic structure factor theory of Doi, Shimada, and Okano[24] to arbitrary time and length scales. Using second-order perturbation theory, we express the primary decay rate observed in dynamic light scattering experiments in a power series of the wave vector, whose coefficients contain diffusion coefficients representing various dynamic processes. Our formulas indicate that, at small wave vectors, DLS probes translational mobility, as we expect. At large wave vectors, the more localized motion (the rotation) is probed also. Because of the geometry-induced anisotropy in the hydrodynamic friction of the translational mobilities, translation is coupled with rotation. This coupling motion makes interpretation of the DLS spectrum difficult at long wave vectors. Our formulas express the influence of this coupling explicitly.

We have measured the rotational relaxation times of our poly(γ-benzyl-α-L-glutamates using transient electric birefringence. CONTIN analysis of the decay in the birefringence signal shows two dynamic modes. One belongs to the rotation, and the other is most likely from the bending motion or the coupling between internal bending and rotation. The measured rotational diffusion coefficients compare favorably with those predicted by the theory of Fixman[21] and the modified caging theory of Keep and Pecora[18] up to 150 rod/L^3 in the context of the dynamic mean field theory.

We have elucidated translational motions of our model systems, suspended in a good solvent mixture, from the DLS spectrum by using our extension of the DSO theory and our knowledge of the rotational diffusion coefficients obtained from the TEB experiments. Within the scope of the mean field approach, we have obtained the diffusion coefficients for mutual diffusion, self-translational diffusion, the translational anisotropy, and the translational self-diffusion coefficients perpendicular and parallel to the rod axis.

CONTIN analysis of the DLS spectrum demonstrates one dynamic mode (first decay rate) at low concentration, and the appearance of another mode at higher concentrations, and large wave vectors. The first mode (slower) is the one that we have intensively investigated in this paper. The behavior and presence of the second mode suggests that it would be useful to probe the rotation-dominated dynamic process because its decay rate decreases with the polymer concentration, consistently with the results from TEB experiment. The first

decay rate of the short rod depends linearly on the square of the wave vector at all concentrations. On the other hand, the first decay rate of the long rod deviates downward from linearity at high concentration and large wave vector.

We have applied our theoretical expression for the major decay rate and demonstrated that the deviation is mainly the result of the rotation-contaminated translational mode. As a consequence, the mutual diffusion coefficient is not the apparent measured diffusion coefficient but the slope of the measured decay rate plotted against wave vector squared in the linear region. The transition from the dilute to the semidilute regimes is observed at about the same concentration as seen in the TEB data. The self-translational diffusion coefficient calculated directly from the mutual value continuously decreases and diverges from the mutual coefficient as the concentration increases. Although the self values are on the same order of magnitude as the results from a tracer experiment,[51] the finding here that they do not remain constant in any concentration range differs from that of the previous investigation. Moreover, self-diffusion coefficients obtained from this approach decrease with polymer concentration at a much slower rate than what was directly measured by Bu et al.[51]

The negative deviations from the linear behavior mentioned above provide information on translational anisotropy. We have found that the translational anisotropy increases sharply with concentration between 40 and 100 rods/L^3. At the larger concentrations studied, we observe very little change in the anisotropy. The abrupt change is due to the large loss in the translational mobility in the perpendicular direction, rather than the parallel motion which remains relatively constant. Although the transverse translational diffusion coefficient is reduced by 95% at 200 rods/L^3, the longitudinal translation has decreased by only 20%. This indicates that the Doi−Edwards assumption of totally limited transverse translation is not valid below 200 rods/L^3. Also, the Fixman model of rotation requiring transverse mobility breaks down at a concentration above this concentration threshold. Indeed, an earlier simulation study reported the break down at a very similar concentration.[23]

Acknowledgment. This work was supported by the National Science Foundation Grant No. CHE 9520845. We are grateful to Dr. Mark A. Tracy for his help in the early stages of this work. Professor Don Eden provided invaluable assistance in setting up the transient electric birefringence apparatus. J. K.P would like to acknowledge helpful discussions with Professor E. S. G. Shaqfeh.

References and Notes

(1) Tracy, M. A.; Pecora, R. *Annu. Rev. Phys. Chem.* **1992**, *43*, 525.
(2) Aharoni, S. M.; Edwards, S. F. *Adv. Polym. Sci.* **1994**, *118*, 1.
(3) Doi, M. *J. Phys.* **1975**, *36*, 607. Doi, M.; Edwards, S. F. *J. Chem. Soc., Faraday Trans. 2* **1978**, *74*, 560; 918.
(4) Doi, M.; Edwards, S. F. *The Theory of Polymer Dynamics*; Oxford University: Oxford, 1986.
(5) Elias, J. G.; Eden, D. *Macromolecules* **1981**, *14*, 410.
(6) Nwammuo, O.; Maitland, G. C. *J. Chem. Soc., Faraday Trans.* **1992**, *88*, 1803.
(7) Newman, J.; Swinney, H. L. *Biopolymers* **1976**, *15*, 301.
(8) O'Konski, C. T. *Molecular Electrooptics. Part 1*; Marcel Dekker: New York, 1976.
(9) Fredericq, E.; Houssier, C. *Electric Dichroism and Electric Birefringence*; Oxford University Press: London, 1973.
(10) Shah, M. J.; Hart, C. M. Investigations of the electrooptical birefringence of polydisperse bentonite suspensions. *IBM J.* (January) 1963.
(11) Hill, D. A.; Soane, D. S. *J. Polym. Sci., Part B: Polym. Phys.* **1989**, *27*, 2295.
(12) Szamel, G.; Schweizer, K. S. *J. Chem. Phys.* **1993**, *100*, 3127.
(13) Mori, Y.; Ookubo, N.; Hayakawa, R.; Wada, Y. *J. Polym. Sci: Polym. Phys. Ed.* **1982**, *20*, 2111.
(14) Watanabe, H.; Yoshioka, K. *Biopolymers* **1964**, *2*, 91.
(15) Oakley, D. M.; Jennings, B. R. *J. Colloid Interface Sci.* **1983**, *91*, 188.
(16) Jennings, B. R.; Nah, M. *J. Colloid Interface Sci.* **1989**, *131*, 47.
(17) Zero, K. M.; Pecora, R. *Macromolecules* **1982**, *15*, 87.
(18) Keep, G. T.; Pecora, R. *Macromolecules* **1985**, *18*, 1167.
(19) Teraoka, I.; Ookubo, N.; Hayakawa, R. *Phys. Rev. Lett.* **1985**, 55, 2712.
(20) Fixman, M. *Phys. Rev. Lett.* **1985**, *54*, 337.
(21) Fixman, M. *Phys. Rev. Lett.* **1985**, *55*, 2429.
(22) Bitsanis, I.; Davis, H. T.; Tirrell, M. *Macromolecules* **1988**, *21*, 2824.
(23) Bitsanis, I.; Davis, H. T.; Tirrell, M. *Macromolecules* **1990**, *23*, 1157.
(24) Doi, M.; Shimada, T.; Okano, K. *J. Chem. Phys.* **1988**, *88*, 4070.
(25) Berne, B. J.; Pecora, R. *Dynamic Light Scattering*; Kreiger: Malabar, FL, 1990.
(26) DeLong, L. M.; Russo, P. S. *Macromolecules* **1991**, *24*, 6139.
(27) Provencher, S. *Comput. Phys. Commun.* **1982**, *27*, 213; 239; *J. Chem. Phys.* **1976**, *64*, 2772.
(28) Maeda, T. *Macromolecules* **1989**, *22*, 1881.
(29) Maeda, T. *Macromolecules* **1990**, *23*, 1644.
(30) Rallison, J. M.; Leal, L. G. *J. Chem. Phys.* **1981**, *74*, 4819.
(31) Russo, P. S.; Karasz, F. E.; Langley, K. *J. Chem. Phys.* **1984**, *80*, 5312.
(32) Wilcoxon, J. P.; Schurr, J. M. *Biopolymers* **1983**, *22*, 849.
(33) Fujime, S.; Takasaki-Oshita, M.; Maeda, T. *Macromolecules* **1987**, *20*, 1292.
(34) Tracy, M. A.; Pecora, R. *Macromolecules* **1992**, *25*, 337. Tracy, M. A.; Garcia, J.-L.; Pecora, R. *Macromolecules* **1993**, *26*, 1862.
(35) Balik, C.; Hopfinger, A. *J. Colliod Interface Sci.* **1978**, *67*, 118.
(36) Phalakornkul, J. K.; Gast, A. P.; Pecora, R.; Nagele, G.; Ferrante, A.; Mandl-Steininger, B.; Klein, R. *Phys. Rev. E* **1996**, *54*, 661.
(37) Phalakornkul, J. K.; Gast, A. P.; Pecora, R. *J. Chem. Phys.* **1999**, submitted for publication.
(38) Pecora, R. *J. Chem. Phys.* **1969**, *50*, 2650.
(39) Lewis, R. J.; Pecora, R.; Eden, D. *Macromolecules* **1986**, *19*, 134.
(40) Lewis, R. J.; Huang, J. H.; Pecora, R. *Macromolecules* **1985**, *18*, 944.
(41) Sorlie, S. S.; Pecora, R. *Macromolecules* **1990**, *23*, 487.
(42) Broersma, S. *J. Chem. Phys.* **1960**, *32*, 1626; 1632; **1981**, *74*, 6989.
(43) Claire, K.; Pecora, R. *J. Phys. Chem.* **1997**, *101*, 746.
(44) Schmidt, M.; Stockmayer, W. H. *Macromolecules* **1984**, *17*, 553.
(45) Maeda, T.; Fujime, S. *Macromolecules* **1984**, *17*, 1157.
(46) Russo, P. S. In *Dynamic Light Scattering, The Method and Some Applications*; Brown, W., Ed.; Oxford: New York, 1992.
(47) Schurr, J. M.; Schmitz, K. S. *Annu. Rev. Phys. Chem.* **1986**, *37*, 271.
(48) Yamakawa, H. *Modern Theory of Polymer Solutions*; Harper and Row: New York, 1971.
(49) Peterson, J. *J. Chem. Phys.* **1964**, *40*, 2680.
(50) Itou, S.; Nishioka, N.; Norisuye, T.; Teramoto, A. *Macromolecules* **1981**, *14*, 904.
(51) Bu, Z.; Russo, P. S.; Tipton, D. L.; Negulescu, I. I. *Macromolecules* **1994**, *27*, 6871.
(52) Kubota, K.; Chu, B. *Biopolymers* **1983**, *22*, 1461.
(53) Szamel, G. *Phys. Rev. Lett.* **1993**, *70*, 3744.
(54) Edwards, S. F.; Evans, K. E. *J. Chem. Soc., Faraday Trans. 2* **1982**, *78*, 113.
(55) Teraoka, I.; Hayakawa, R. *J. Chem. Phys.* **1988**, *89*, 6989.
(56) Sato, T.; Teramoto, A. *Macromolecules* **1991**, *24*, 193.
(57) Enomoto, H.; Einaga, Y.; Teramoto, A. *Macromolecules* **1985**, *18*, 2695.
(58) Yamakawa, H. *Annu. Rev. Phys. Chem.* **1984**, *35*, 23.
(59) Roitman, D. B.; Zimm, B. H. *J. Chem. Phys.* **1984**, *81*, 6248; 6333; 6356.

MA981640D